Korean J. Chem. Eng., 40(5), 1176-1185 (2023)
DOI: 10.1007/s11814-022-1365-z

pISSN: 0256-1115
eISSN: 1975-7220

Ionic liquid functionalized graphene oxide for the adsorption of Ca^{2+} and Mg^{2+} ions from saline aqueous feed

Botagoz Zhuman*,, Hadil Abu Khalifeh*, Ioannis Zuburtikudis*,†, Mahendra Kumar**, Hassan A. Arafat**, and Enas Nashef****

*Chemical Engineering Department, Abu Dhabi University, P.O. Box 59911, Abu Dhabi, U.A.E.
**Center for Membrane and Advanced Water Technology, Khalifa University, P.O. Box 127788, Abu Dhabi, U.A.E.
(*Received 30 July 2022 • Revised 2 December 2022 • Accepted 4 December 2022*)

Abstract−The development of an efficient adsorbent for removal of Ca^{2+} and Mg^{2+} ions using ionic liquid (IL) (1-Ethyl-3-methylimidazolium amino acetate) functionalized graphene oxide (GO) (IL-GO) is reported. The formation of IL-GO adsorbent was confirmed by FTIR, Raman, TGA, TEM and SEM-EDX analysis. The loading of IL within the IL-GO adsorbent was found to be 39 wt%. A minimum amount of IL (~2%) leached from IL-GO after continuous stirring in DI water for 24 h. The IL-GO adsorbent exhibited high adsorption capacity towards Ca^{2+} and Mg^{2+} ions and stable recovery without cross-contamination of the feed water. The structural integrity of IL-GO was preserved after functionalization and adsorption of Ca^{2+} and Mg^{2+} from aqueous solution. Adsorption kinetics results show that the adsorption rates of Ca^{2+} and Mg^{2+} follow a pseudo second-order kinetic model. Moreover, the adsorption data of both Ca^{2+} and Mg^{2+} on IL-GO is well fitted using the Langmuir isotherm, implying that active sites for adsorption are homogeneously distributed on the IL-GO surface. IL-GO adsorbent shows promise in the removal of Ca^{2+} and Mg^{2+} ions from saline water, as part of a pretreatment process in reverse osmosis (RO) desalination plants, to control the inorganic fouling of RO membranes. Finally, since the adsorption capacity of IL-GO for Ca^{2+} and Mg^{2+} has been found to be much greater than that for Na^{+}, the developed adsorbent could be a very good candidate for the separation of monovalent and divalent cations from an aqueous feed.

Keywords: Graphene Oxide, Ionic Liquid, Adsorption, Ca^{2+} and Mg^{2+}, Membrane Fouling, Desalination

INTRODUCTION

Graphene (GN), which consists of sp^2 hybridized carbon atoms bonded together with a bond length of 0.142 nm [1], has received a significant consideration because of its versatility. GN is oxidized easily to produce graphene oxide (GO). The oxygen containing functional groups on the basal plane of GO act as reactive sites for further modification *via* various chemical reactions [2,3]. Nanostructured GO has been applied as an adsorbent for the removal of heavy metal ions from aqueous solutions and wastewater [4]. The adsorption capacity of GO for heavy metal ions is much higher than carbon nanotubes (CNTs) and activated carbon (AC) [3]. However, limited research has been conducted on the usage of GO in the removal of alkali and alkaline earth metal ions (Na^{+}, Ca^{2+} and Mg^{2+}) through adsorption [5-7]. Despite being an excellent adsorbent of different metal ions and pollutants, GO is difficult to recycle due to challenges in its recovery from the feed water [4,8,9]. It is, therefore, of great interest to design nanostructured GO-based adsorbents for the removal of alkaline bi-valent metal ions with easy post-use solid-liquid separation efficacy.

Today, the development of robust, ecofriendly processes for the removal of salts from seawater is of high priority. Membrane-based desalination processes, such as reverse osmosis (RO), are applied on large scale for salt removal from seawater [10]. However, RO is considered costly, with membrane fouling being one reason behind this cost. One type of fouling, the so-called inorganic fouling or scaling, occurs due to the deposition of inorganic salts on the membranes. In particular, calcium and magnesium salts are deposited on the membrane surface at high feed pressure [11,12]. Therefore, pre-treatment of feed seawater containing Ca^{2+} and Mg^{2+} using efficient adsorbents can be effective in addressing the membrane scaling problem.

Ionic liquids (ILs) have been explored as eco-efficient solvents in water treatment for the extraction of different metal ions from water [6,13,14]. However, cross-contamination of feed water could occur during metal ions extraction. This cross-contamination risk can be mitigated via the immobilization of ILs on suitable support material. Recently, nanostructured GO was tested as a potential support material for the immobilization of ILs via chemical modification [15]. IL-modified GO adsorbents, which have additional functional groups on their surface, have exhibited enhanced affinity towards toxic contaminants in aqueous solution and improved recoverability [16]. However, the immobilization of ILs onto the surface of nanostructured GO by chemical modification needs to be stable to avoid the leaching of ILs into the feed water. Covalent immobilization of ILs onto nanostructured materials can be achieved via acylation, esterification, isocyanate formation, nucleophilic ring opening, amide formation, diazotization and cycloaddition reactions [17].

In this study, a new IL-functionalized GO (IL-GO) adsorbent

†To whom correspondence should be addressed.
E-mail: ioannis.zuburtikudis@adu.ac.ae

was prepared via an epoxide ring opening reaction and amidation at 80 °C using a specific IL (1-Ethyl-3-methylimidazolium amino acetate) for the adsorption of Ca^{2+} and Mg^{2+} ions from aqueous solution. It is hypothesized that the adsorption capacity of modified GO after functionalization with IL can be enhanced for alkaline earth metal ions due to the creation of extra active adsorption sites without cross-contamination of feed water with IL [18]. In addition, IL-GO adsorbent can be easily isolated from the feed water via filtration. The produced IL-GO adsorbent is expected to have high adsorption capacity for Ca^{2+} and Mg^{2+} ions, enabling its application in the pretreatment of RO feed to prevent the inorganic fouling of RO membranes. To the best of our knowledge, a specific IL functionalized GO (IL-GO) adsorbent is used herein for the first time for adsorption of Ca^{2+} and Mg^{2+} ions. The IL-GO adsorbent was characterized thoroughly and the impact of various parameters, including contact time, solution pH, adsorbent dose and temperature, on the adsorption process was studied.

EXPERIMENTAL

1. Materials

Ionic liquid (IL) (1-Ethyl-3-methylimidazolium amino acetate (>97%)), graphite, potassium hydroxide (KOH), potassium permanganate ($KMnO_4$), sulfuric acid (H_2SO_4, 96%), hydrochloric acid (HCl, 36.5%), hydrogen peroxide (H_2O_2) and absolute ethanol were procured from Sigma-Aldrich. $MgCl_2$ and $CaCl_2$ were purchased from Acros Chemicals. Deionized (DI) water was used in the preparation of all solutions, while GO was synthesized in our lab following a previously reported protocol [19] and is presented below.

2. Synthesis of GO

GO was synthesized in our lab according to the modified Hummers method [5]. Initially, 2 g of graphite flakes was charged into a 2 L media glass bottle containing 250 mL H_2SO_4 under constant mechanical stirring of 300 rpm. The resulting mixture was further stirred for 2 h and 15 g of $KMnO_4$ was gradually added into the suspension, which was left overnight at a stirring speed of 300 rpm. The color of the mixture turned to purple after 1 h heating at 80 °C. Then, the temperature of the mixture was dropped to room temperature (RT) and 200 mL of DI water was added dropwise into the mixture over 2 h under the ice-cold condition at high mechanical stirring. Thereafter, 100 mL of H_2O_2 was added into the resulting mixture, which was left overnight at room temperature without stirring. The supernatant solution was discarded and oxidized graphite was washed with 200 mL of 10 wt% HCl. Then, the suspension was centrifuged with DI water until the pH of supernatant solution reached to 5.5. A brown color paste was isolated from the centrifuge tubes and was subsequently dispersed in absolute ethanol using a bath sonicator. The centrifugation and dispersion steps were repeated three times to eradicate the remaining impurities from GO suspension and purified GO suspension in ethanol was transferred onto glass petri dish and left inside airflow-controlled fume cupboard overnight at RT. The dried GO was taken out from the glass petri dish and stored in a Ziplock plastic bag for characterization and further use in preparation of IL-GO adsorbent.

3. Preparation of Ionic Liquid Functionalized GO

IL-functionalized GO (IL-GO) adsorbent was prepared by an epoxide ring opening and amidation reaction at 80 °C using GO sheets and IL (1-Ethyl-3-methylimidazolium amino acetate) (Fig. 1). Initially, a well-dispersed suspension of GO in DI water (0.5 mg mL^{-1}) was prepared by adding 500 mg of GO into one neck round bottom flask containing 1,000 mL DI water and the dispersion of mixture was carried out in a bath sonicator for 30 min. Then, 1 g of IL and 250 mg of KOH were alternatively charged into the well-dispersed suspension of GO in water under constant stirring. The alkaline mixture of GO in water was further sonicated over 30 min, after which the pH was adjusted to 10 by adding few drops of 2 M HCl. The flask, along with the GO mixture, was immersed into a preheated oil bath and the refluxing continued at 80 °C for 24 h. The resulting suspension was cooled to room temperature and, subsequently, centrifugation was carried out at 8,000 rpm for 30 min to obtain a black paste, which was re-dispersed in ethanol for 30 min in the bath sonicator. A suspension of modified GO was centrifuged and sonicated alternately in ethanol twice for the removal of impurity traces. The purified black paste of IL-GO was again dispersed in ethanol and transferred into a large glass petri-dish. The petri-dish, with the IL-GO suspension, was kept in an airflow-controlled fume cupboard overnight at room temperature. The dried IL-GO was then removed from the petri dish using a spatula and immediately stored in a Ziplock plastic bag before characterizations and later use.

4. Adsorbent Characterization

The surface morphology of GO and IL-GO was investigated using

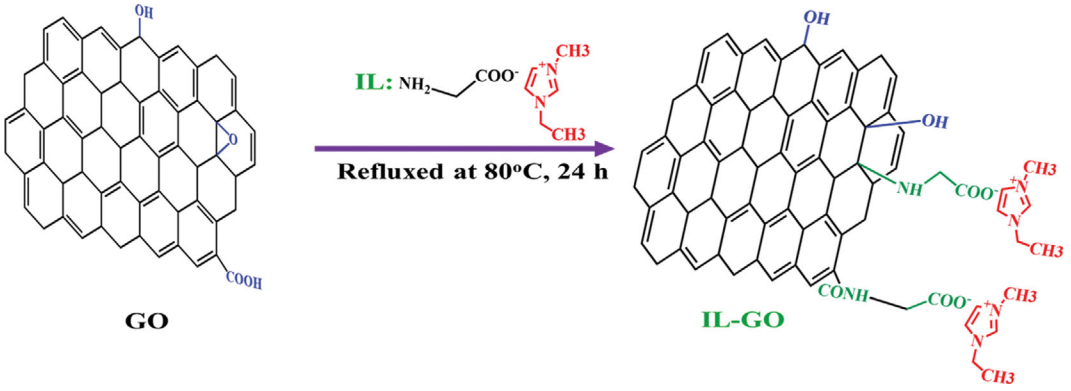

Fig. 1. Schematic of the synthesis route of IL-functionalized GO (IL-GO) via epoxide ring opening and amidation reaction at 80 °C.

a high-resolution scanning electron microscope (SEM) (Nova Nano, FEI) linked to energy-dispersive X-ray analysis probe (EDXS, FEI, The Netherlands). Both GO and IL-GO samples in powder form were first immobilized atop SEM stubs using a prefixed double-sided carbon tape. Then, the samples were coated with a 10 nm layer of Au-Pd layer under vacuum using a sputtering machine. SEM images of both samples were recorded at 10 μm scanning scale. SEM-EDX spectra before and after adsorption of Ca^{2+} and Mg^{2+} ions onto GO and IL-GO were also recorded.

HR-TEM images of GO and IL-GO samples were taken using a transmission electron microscope (TEM) (Tecnai G2 series, FEI) to examine the structural changes of GO sheets after IL functionalization. For that, a dried powder sample of GO or IL-GO was initially dispersed in ethanol at 100 μg mL^{-1} concentration using a bath sonicator for 30 min. The liquid suspension was then dropped on TEM grids and subsequently ethanol was removed in an airflow-controlled fume-cupboard at room temperature. TEM images were then acquired at 20 nm scanning scale. Wide angle X-ray diffraction (WAXRD) analysis of GO and IL-GO was performed on a Bruker D2 Phaser X-ray diffractometer with Cu K_α radiation source (λ= 1.54 Å). WAXRD spectra were collected at a step size of 0.0167 and the interlayer spacing (d) was calculated using Bragg's Law (2d sin θ=nλ).

ATR-FTIR spectra were obtained in the range of 4,000 to 460 cm^{-1} at a resolution of ±4 for 64 scans using an attenuated transform reflection-Fourier transform infrared (ATR-FTIR) spectrometer (VERTEX, 80/80v, Germany). Raman spectra were recorded using a Raman spectrometer (Renishaw Invia, UK) at 540 nm wavelength. Thermogravimetric analysis (TGA) was done using a Netzsch STA 449 F3 Jupiter TGA instrument. TGA data was acquired in the temperature range of 50 to 800 °C at a 10 °C min^{-1} heating rate under N_2 flow.

5. Quantification of IL Leaching

Initially, 15 mg of IL-GO was added into a conical flask containing 30 mL of DI water, which was then sonicated in a bath sonicator for 10 min. The conical flask, containing a well-dispersed suspension of IL-GO, was then placed on a mechanical shaker and stirred at 300 rpm for 24 h. The suspension was filtered using vacuum filtration and the supernatant solution was stored in airtight glass bottle before analysis. A total carbon content (TOC) analyzer (TOC-LCSH/CSN, Shimadzu, Japan) was used in determining the TOC of the supernatant solution. The leaching of IL from IL-GO adsorbent was calculated as:

$$\text{Leaching}\ (\%) = \frac{\Delta TOC \times V_s \times C_{IL}}{m_{IL}} \times 100 \quad (1)$$

where ΔTOC is the difference in TOC (mg L^{-1}) between the supernatant solution (after IL leaching) and DI water (before leaching), V_s is the total volume of water (L), m_{IL} is the weight of IL in the leached IL-GO sample (mg) and C_{IL} is the content of carbon in IL (mg).

6. Adsorption Studies

Batch adsorption tests were carried out for the adsorption of Na^+, Ca^{2+} and Mg^{2+} from aqueous solutions using IL-GO adsorbent. A specific amount of IL-GO was added into an individual solution of NaCl, $CaCl_2$ or $MgCl_2$ in a 50 mL conical flask and stirred on an incubator shaker at 100 rpm for a predetermined time. After that, the supernatant solution was filtered using a syringe filter (Agilent, 0.2 μm, Cellulose acetate) and the concentration of Na^+, Ca^{2+} or Mg^{2+} ions was determined using an inductively coupled plasma-optical emission spectrometer (ICP-OES Model 5100 SVDV, Agilent, USA). Adsorption studies were also carried out by varying the concentration of metal ions in solution, adsorption time, adsorbent mass, temperature and solution pH. The adsorption capacity (q_e) of IL-GO at equilibrium was calculated as:

$$q_e (\text{mg g}^{-1}) = \frac{(C_0 - C_e) \times V}{m} \quad (2)$$

where C_0 is the initial concentration of metal ion (mg L^{-1}), C_e is the equilibrium concentration (mg L^{-1}), V is the total volume (L); and m is the weight of adsorbent (g).

RESULTS AND DISCUSSION

1. Physico-chemical Characterization of GO and IL-GO

The ATR-FTIR spectra of GO, IL, and IL-GO are shown in Fig. 2 and a tabulation of the characteristic peaks present in these spectra is provided in Table S1 (Supplementary Information, SI)). The characteristic peaks in the FTIR spectrum of GO are associated as: sp^2 aromatic C=C vibration at 1,622 cm^{-1}, oxygen containing functional groups such as carbonyl C=O stretching at 1,729 cm^{-1}, C-O-C bending at 1,225 cm^{-1}, C-OH group at 1,391 cm^{-1}, C-O stretching vibration at 1,060 cm^{-1}, and O-H stretching vibrations at 3,350 cm^{-1}) [20,21]. The stretching vibration of O-H seems to be flattened in the FTIR spectrum of IL-GO, which suggests that GO was partially reduced. New peaks for C-O at 1,171 cm^{-1}, and C-H bond at 620 cm^{-1} are observed in IL-GO, while an intense peak for C-N at 1,288 cm^{-1} and -NH at 3,158 cm^{-1} in the spectrum of IL-GO validates the functionalization of GO with IL after amidation and epoxide ring opening reaction at 80 °C [22]. The peaks for C=O in the FTIR spectrum of IL-GO also suggest the presence of

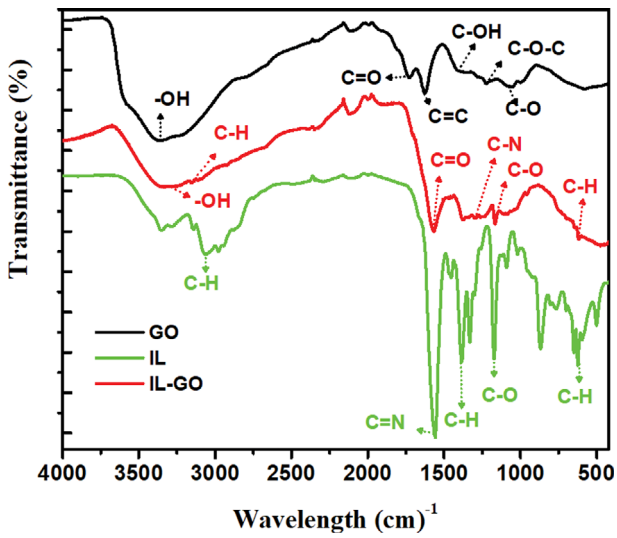

Fig. 2. ATR-FTIR spectra of GO, IL and IL-GO in the range of 4,000 to 460 cm^{-1}.

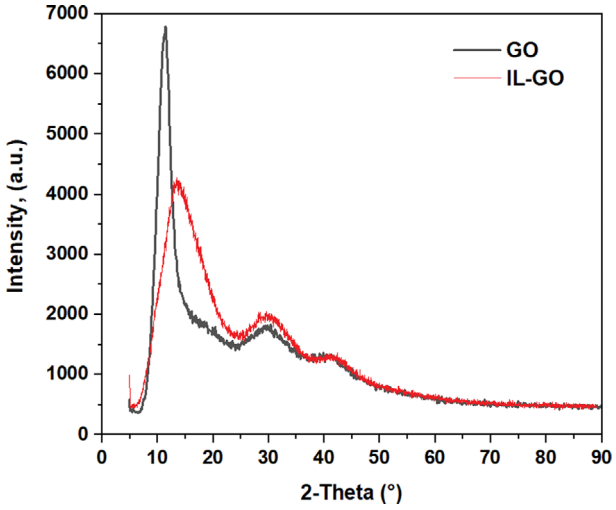

Fig. 3. WAXRD patterns of GO and IL-GO in the range of 5 to 90° at a step size of 0.0167.

acetate anion within IL-GO. In addition, the characteristic peaks for C=N at 1,565 cm^{-1}, C-H bending at 1,378 cm^{-1}, C-O stretching at 1,167 cm^{-1}, and C-H at 3,059 cm^{-1} are seen in the FTIR spectrum of IL (Table S1) [23,24].

WAXRD patterns of GO and IL-GO are displayed in Fig. 3. The peaks at 2θ=29.6° and 2θ=41.5° correspond to (002) and (100) lattices of non-oxidized traces of graphitic structure in GO and IL-GO, respectively [25]. The characteristic peak at 2θ=11.48° links to (002) crystal plane of GO. This peak became broad and shifted to 2θ=13.76° for IL-GO, while its intensity was reduced. Also, the interlayer distance was reduced from 0.77 (GO) to 0.64 nm after functionalization of GO with IL. The peak broadening and reduction in interlayer distance after IL functionalization could be attributed to the delamination of GO by ultrasound waves [21]. According to Scherrer's equation ($W_{FWHM}=\frac{m\lambda}{T\cos\theta}$ where W_{FWHM} is the peak broadening at full width half maximum (FWHM), m is a constant, λ is the X-ray wavelength, T is the thickness of the crystal plane and θ is the Bragg diffraction angle (deg.)), the thickness of the crystal plane is inversely proportional to the peak broadening and, therefore, the modified GO had less thickness, which might be attributed to the reduction in aggregation of GO sheets with the introduction of IL and stearic hindrance between IL molecules on the surface of GO [26].

Raman spectra for GO and IL-GO are depicted in Fig. 4. The characteristic G band is related to sp^2-bonded carbon atoms within the hexagonal lattice of GO and IL-GO. The characteristic D band reflects the presence of defects or disorders because of sp^3 hybridized carbon in the lattice, while 2D (G') band is caused by second-order zone boundary phonons that are associated with the assembly of multilayers [25]. The intensity ratio of D and G bands (I_D/I_G) provides an indication for the degree of oxidation and/or functionalization of GO nanosheets [25,27]. The I_D/I_G ratio increased from 0.90 (GO) to 0.97 after functionalization of GO with IL, due to the creation of more defects and the number of functional groups

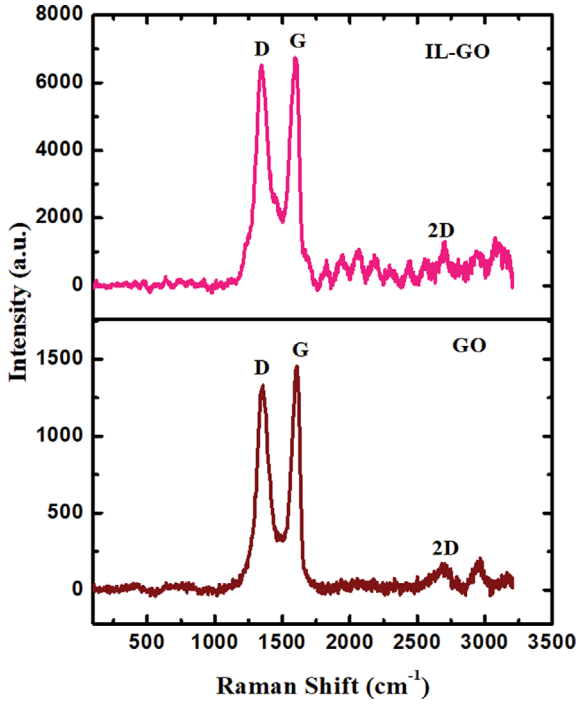

Fig. 4. Raman spectra of GO and IL-GO in the range of 500 to 3,000 cm^{-1}.

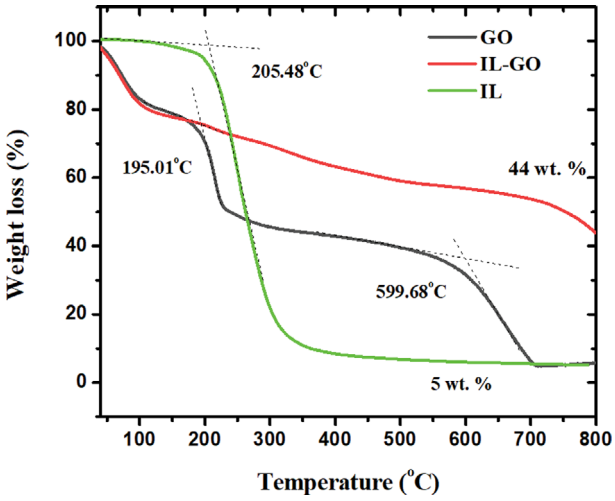

Fig. 5. TGA data of GO, IL and IL-GO in the temperature range of 50 to 800 °C at 10 °C min^{-1}.

on the surface of IL-GO.

TGA data of GO, IL and IL-GO are shown in Fig. 5. A one decomposition step is observed for IL at 205.5 °C. Two steps of decomposition can be observed for GO at onset decomposition temperatures of 195 °C and 599.7 °C. IL-GO also displayed a two-step decomposition, but at 120 °C and 680 °C. However, the decomposition rate of IL-GO at high temperature was slower in comparison to GO under identical conditions. This can be associated with a partial reduction of GO in an alkaline medium and the subsequent introduction of low T_g aminated IL (1-Ethyl-3-methylimidazolium amino acetate) onto the surface of GO upon covalent func-

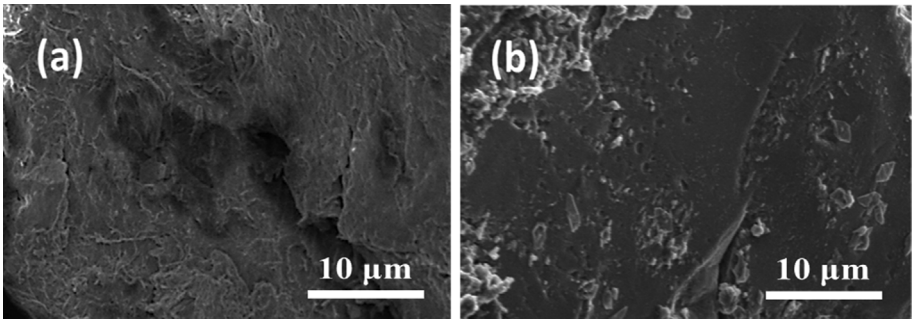

Fig. 6. High resolution SEM images of: (a) GO and (b) IL-GO.

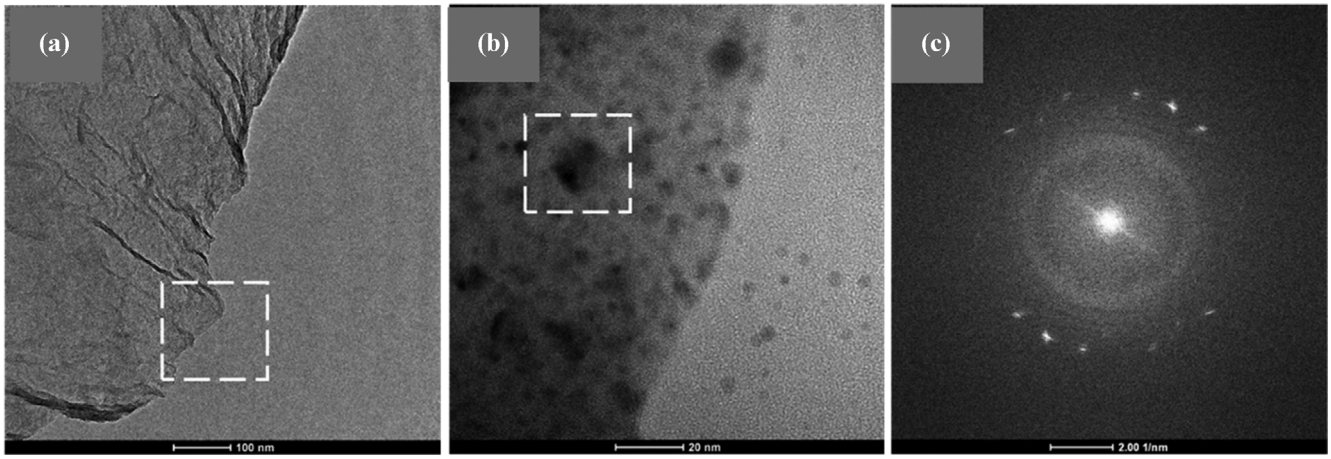

Fig. 7. TEM images of (a) GO, (b) IL-GO and (c) SAED pattern of IL-GO at 2.0 nm scanning scale.

tionalization. The loading amount of IL within IL-GO was determined as the difference in weight of GO and IL-GO residues left at 800 °C [20], and was found to be 39%.

2. Morphological Characterization of GO and IL-GO

An alteration in surface texture of GO after functionalization with IL was detected by recording their high-resolution SEM images shown in Fig. 6. The surface texture of GO is characterized by stacked layers (Fig. 6(a)), while in case of IL-GO, the surface texture is porous and rougher (Fig. 6(b)). Additionally, the SEM image of IL-GO indicates that more defects were created within the GO surface upon its functionalization with IL.

Fig. 7 depicts the TEM images of GO and IL-GO at scanning scale of 100 and 20 nm, respectively. TEM image of the former indicates that GO had almost transparent layer with wrinkled edges (Fig. 7(a)), while TEM image of the latter show uniformly black spots distributed within the texture of IL-GO (Fig. 7(b)), as ILs are salts which are inherently crystalline. The selected area of electron diffraction (SAED) pattern signifies the polycrystalline structure of IL-GO (Fig. 7(c)).

3. Leaching of IL from IL-GO

The cross-contamination of feed water by IL leaching out from the adsorbent during water treatment is highly undesirable. Therefore, the leaching of IL from IL-GO was quantified in this study by determining the TOC content of the supernatant solution left after IL-GO immersion and stirring in DI water for 24, according to a protocol reported by Pirkwieser et al. [28]. A limited number of studies quantify and report the issue of IL leaching, though it is critical to consider leaching when using the adsorbent in water treatment applications [29]. TOC results of the supernatant solution identified that only 2 wt% of IL was leached into the feed water over 24 h. Taking into consideration the hydrophilicity of the IL, the observed 2% IL leaching from the IL-GO matrix is considered to be low. This low tendency of IL to leach out of IL-GO suggests that the chances for cross-contamination of feed water by IL-GO can be assumed negligible during the application of IL-GO in the adsorption of alkaline earth metal ions from aqueous solution.

4. Key Thermodynamic Properties of Ca^{2+} and Mg^{2+} Adsorption on IL-GO

Three key thermodynamic parameters of relevance to the adsorption of Ca^{2+} and Mg^{2+} on IL-GO were determined. These are the changes in Gibbs free energy (ΔG^o), enthalpy (ΔH^o), and entropy (ΔS^o). To accomplish this, the adsorption of Ca^{2+} and Mg^{2+} ions on IL-GO was studied at three temperatures, 25, 35, and 45 °C, at fixed initial salt ion concentration in the feed solution (300 ppm for Ca^{2+}, 500 ppm for Mg^{2+}). For each temperature and at equilibrium, K_C was calculated using the following equations [30]:

$$K_C = \frac{C_{AC}}{C_e} \tag{3}$$

where K_c is the equilibrium constant, C_{AC} and C_e are the equilibrium concentrations of metal ion on the adsorbent and in solution, respectively. From the K_C value, ΔG^o was calculated as:

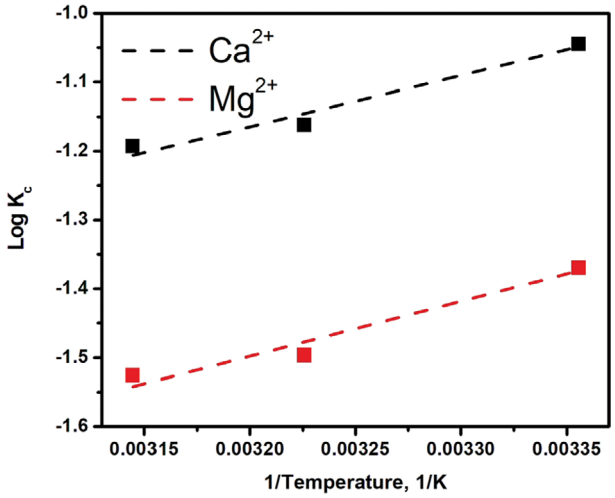

Fig. 8. Van't Hoff plot (log K_c versus 1/T) for Ca^{2+} and Mg^{2+} ions.

$$\Delta G^o = -2.303RT\log K_c \quad (4)$$

where T is the absolute temperature (K) and R is the universal gas constant (R=8.31446 m^3 Pa K^{-1}). Then, ΔS^o and ΔH^o were obtained, respectively, from the slope and intercept of the van't Hoff plot (log K_c versus 1/T), as shown in Fig. 8, based on the following equation [30]:

$$\log K_c = \left(\frac{\Delta S^o}{2.303R}\right) - \left(\frac{\Delta H^o}{2.303RT}\right) \quad (5)$$

The values of all three parameters, tabulated in Table 1, confirmed an exothermic and non-spontaneous adsorption of Ca^{2+} and Mg^{2+} onto IL-GO at all temperatures. The negative values of ΔS^o suggested a decrease in the randomness at the solid-solution interface during adsorption of Ca^{2+} and Mg^{2+} ions [31].

Table 1. Thermodynamic parameters (ΔS^o, ΔH^o and ΔG^o) and correlation coefficient (R^2) of the van't Hoff plot

T (°C)	ΔS^o (J K^{-1} mol^{-1})	ΔH^o (J mol^{-1})	ΔG^o (J mol^{-1})	R^2
Ca^{2+}				
25	−66.25	−13,749.6	5,960.7	0.964
35			6,850.0	
45			7,260.3	
Mg^{2+}				
25	−75.23	−14,565	7,814.5	0.955
35			8,823.8	
45			9,289.0	

5. Kinetics and Equilibrium of Ca^{2+} and Mg^{2+} Adsorption on IL-GO

Fig. 9(a) shows the effect of contact time on the adsorption capacity of IL-GO for Ca^{2+} and Mg^{2+} ions from a feed solution with initial concentration of 150 ppm salt and pH=7. The adsorption capacity starts to plateua after about 2 h, at which point equilibrium is almost reached.

The rate constants for adsorption kinetics were calculated using pseudo first-order and second-order kinetic models [32,33]. The first-order kinetic model is represented as follows (6):

$$\log(q_e - q_t) = \log q_e - \frac{k_1}{2.303}t \quad (6)$$

where q_e is the adsorption capacity of IL-GO ($mg_{ADS}/g_{IL\text{-}GO}$) at equi-

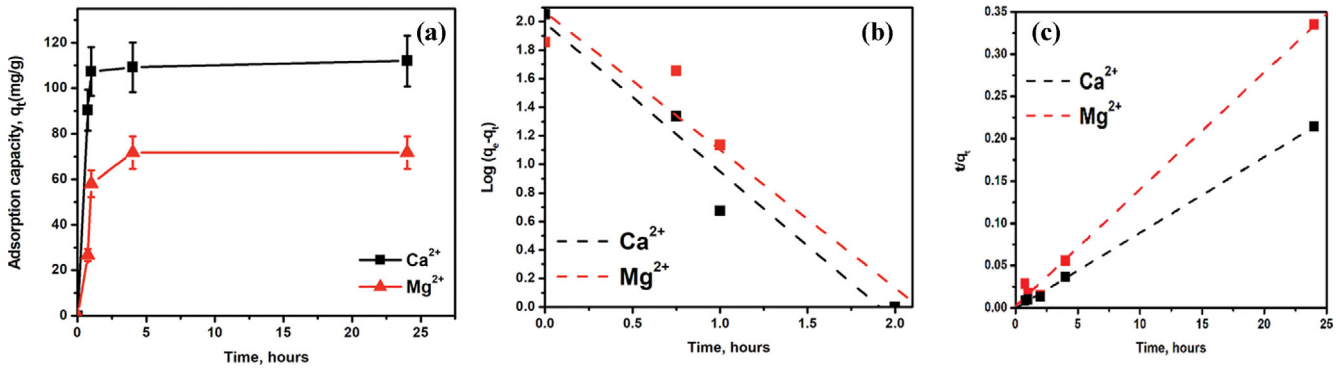

Fig. 9. (a) Effect of contact time on the adsorption capacity of IL-GO at pH=7, (b) pseudo-first-order kinetics plot for adsorption of Ca^{2+} and Mg^{2+} at pH=7, (c) second-order kinetics plot for adsorption of Ca^{2+} and Mg^{2+} at pH=7.

Table 2. Pseudo first-order and second-order kinetic rate constants (k_1, k_2), calculated q_e values and R^2 values for adsorption of Ca^{2+} and Mg^{2+} on IL-GO at pH=7 and initial salt concentration ca. 200 ppm

	Pseudo 1st-order kinetic model			q_e, experimental ($mg_{ADS}/g_{IL\text{-}GO}$)	Pseudo 2nd-order kinetic model		
	R^2	k_1 (min^{-1})	$q_{e,\,pseudo\text{-}1st}$ ($mg_{ADS}/g_{IL\text{-}GO}$)		$q_{e,\,pseudo\text{-}2nd}$ ($mg_{ADS}/g_{IL\text{-}GO}$)	k_2 ($g_{IL\text{-}GO}$ mg_{ADS}^{-1} min^{-1})	R^2
Ca^{2+}	0.9553	0.0398	97.77	112	112.36	0.0012	0.9999
Mg^{2+}	0.9226	0.0370	116.57	71.68	72.46	0.00127	0.9938

librium, q_t is the adsorption capacity after a particular adsorption time, t, and k_1 (min^{-1}) is the rate constant for first-order kinetic model, which is determined from the slope of log ($q_e - q_t$) versus time (t) plot (Fig. 9(b)). The $q_{e,pseudo\text{-}1st}$, k_1 and R^2 values are given in Table 2.

The second-order kinetic model is described as follows [32,33]:

$$\frac{t}{q_t} = \frac{1}{h} + \left(\frac{1}{q_e}\right)t \quad (7)$$

where $h=k_2q_e^2$ and is calculated from the intercept of the t/q_t versus t straight line with the t/q_t axis. k_2 is the rate constant of pseudo second-order kinetics and is calculated through h and the slope of the t/q_t versus t line, as shown in Fig. 9(c). The $q_{e,pseudo\text{-}2nd}$, k_2 ($g_{IL\text{-}GO}$ mg_{ADS}^{-1} min^{-1}) and R^2 values are included in Table 2; note that (mg_{ADS}) refers to the amount (mg) of adsorbed species, either metal cation, on the adsorbent IL-GO. It is noticed that the R^2 values for pseudo second-order kinetics are significantly closer to 1 than the R^2 values for pseudo first-order kinetics for both metal ions. In addition, the calculated q_e values from the pseudo second-order model are very close to the experimental values of q_e for both metal cations, while the ones calculated from the pseudo first-order model are not close to the experimental q_e values. All these results indicate that the adsorption process is much more accurately described by the pseudo second-order model for both cations. The second-order kinetics indicate that the adsorption of both metal ions (Ca^{2+} and Mg^{2+}) on IL-GO is mainly governed by chemisorption.

Insight into the type of prevailing equilibrium isotherm was obtained from a linear fit of equilibrium adsorption data of Ca^{2+} and Mg^{2+} on IL-GO using the Langmuir (Eq. (8)) and Freundlich (Eq. (9)) isotherms [32,33]:

$$\frac{C_e}{q_e} = \frac{1}{K_L} + \frac{a_L}{K_L}C_e \quad (8)$$

$$\log q_e = \log K_F + \frac{1}{n}\log C_e \quad (9)$$

where C_e is the concentration of metal ion in solution at equilibrium, K_L and a_L are Langmuir constants, K_F is Freundlich constant, and 1/n is the heterogeneity factor. K_L and a_L values were obtained from the Langmuir isotherm plots (Fig. 10(a)) and K_F was determined from the Freundlich isotherm plot (Fig. 10(b)). These values, along with the correlation coefficient (R^2), are presented in Table 3. Higher R^2 in case of both metal ions (Ca^{2+}: 0.999 and Mg^{2+}: 0.9998) were obtained for Langmuir isotherm. These values indicate a quick reduction in the intermolecular forces with distance for monolayer adsorption and a homogeneous distribution of the active cites on IL-GO [16]. On the other hand, the lower R^2 values obtained for the data fit using Freundlich isotherm indicate that the adsorption of both metal ions does not match well the characteristics of a heterogeneous adsorption system. The a_L values lying between 0 and 1 ($0<a_L<1$) suggest that the adsorption of both metal ions onto IL-GO was reversible. The q_{max} values calculated from the Langmuir isotherm model for Ca^{2+} and Mg^{2+} ions are 125 and 73 mg g^{-1}, respectively.

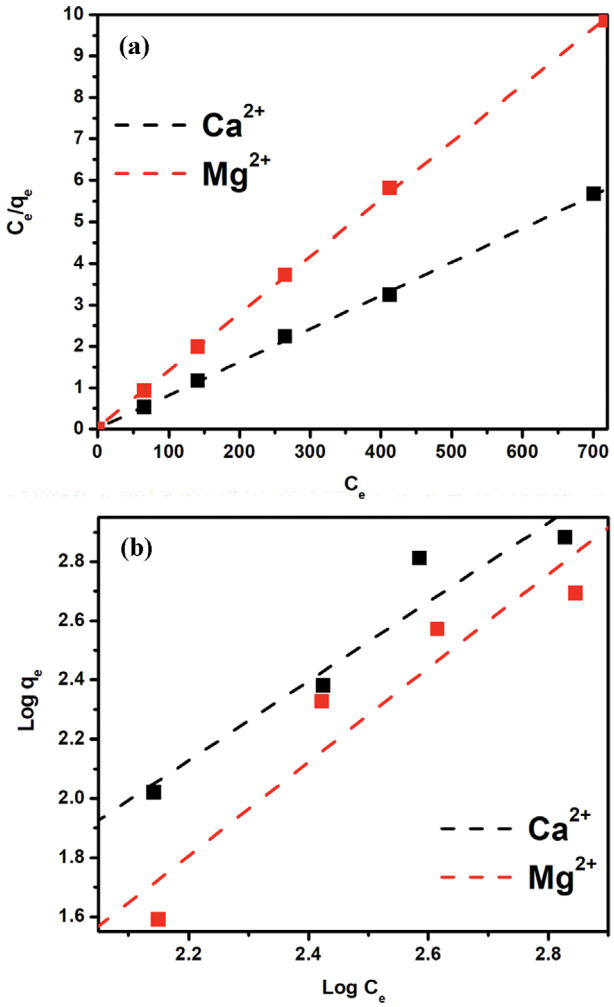

Fig. 10. (a) Langmuir and (b) Freundlich isotherms for the adsorption of Ca^{2+} and Mg^{2+} on IL-GO.

Fig. 11 shows the effect of pH on the adsorption capacity of IL-GO for Ca^{2+} and Mg^{2+}. The highest adsorption of both ions was at pH=5. This is due to the deprotonation of O-H groups of IL-GO at pH>4, resulting in increased electrostatic attraction interactions between the negatively charged functional moieties of IL-GO and the positively charged Ca^{2+} and Mg^{2+} ions at pH>4 [8]. It has been

Table 3. Parameters of Langmuir and Freundlich isotherms as obtained from the best fit of adsorption equilibrium data (Fig. 10)

	Langmuir isotherm				Freundlich isotherm		
	a_L (L/mg_{ADS})	K_L ($L/g_{IL\text{-}GO}$)	q_{max} ($mg_{ADS}/g_{IL\text{-}GO}$)	R^2	K_F $(mg_{ADS}/g_{IL\text{-}GO})/(mg_{ADS}/L)^{(1/n)}$	n	R^2
Ca^{2+}	0.311	38.91	125	0.9989	0.1524	0.7469	0.9197
Mg^{2+}	0.209	14.81	73	0.9998	0.0208	0.6308	0.8954

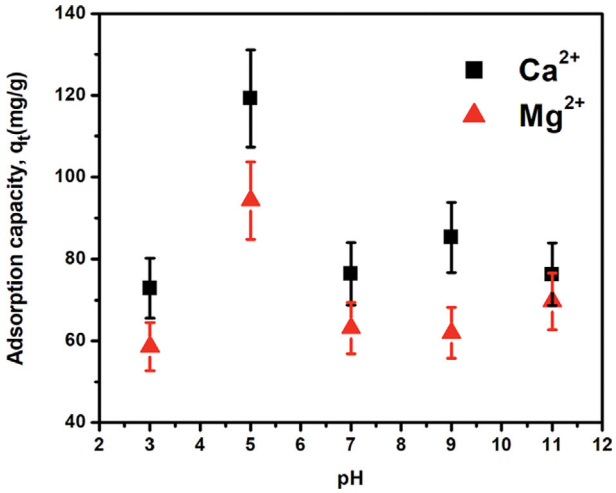

Fig. 11. The effect of pH on the adsorption capacity (q_t: mg g^{-1}) of Ca^{2+} and Mg^{2+} on IL-GO.

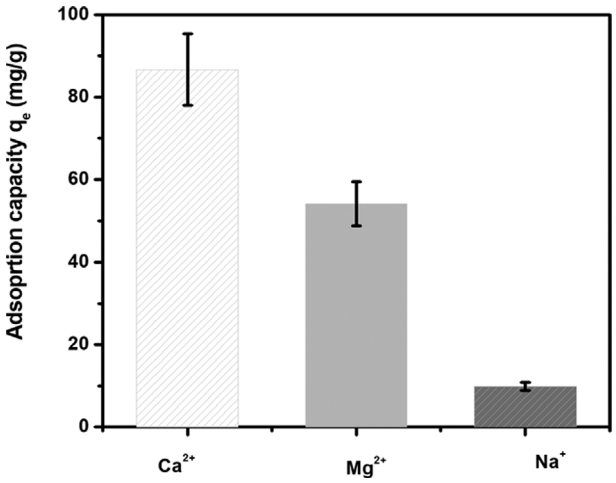

Fig. 12. Comparative adsorption capacity of IL-GO for adsorption of Na^{+}, Ca^{2+} and Mg^{2+}.

reported previously that the charge nature of GO and IL is influenced by changes in pH during adsorption [33,34]. The adsorption capacity of IL-GO for both ions decreased with further increase in pH, from 5 to 11. These changes can be related to the type of cation, the charge of adsorbate solution, and the charge on the surface of adsorbent during adsorption in this pH range [8]. At pH>5, Ca^{2+} was converted into its hydroxide form, which could not be adsorbed in excess by the more negatively charged IL-GO in alkaline medium and, therefore, the adsorption capacity of IL-GO for Ca^{2+} decreased.

The adsorption capacity of IL-GO for Na^{+} was also checked and compared with that for Ca^{2+} and Mg^{2+} (Fig. 12). The q_t of IL-GO for Na^{+} was 10 mg g^{-1} (at initial salt concentration of 250 ppm, pH=7, and T=25 °C), which is much lower than q_t for Ca^{2+} and Mg^{2+} (Ca^{2+}: 87 mg g^{-1} and Mg^{2+}: 54 mg g^{-1}). These results demonstrate that the IL-GO adsorbent was more competent for the adsorption of bivalent inorganic metal ions (Ca^{2+} and Mg^{2+}). For this reason, IL-GO can be considered as a potential adsorbent in the pretreatment of seawater to minimize inorganic fouling of the RO membranes used in desalination. Note that the efficacy of IL-GO needs to be evaluated further using real seawater that contains multiple cations, which is planned as a future work. In addition, since the adsorption capacity of IL-GO for Ca^{2+} and Mg^{2+} has been found to be much greater than that for Na^{+}, the developed adsorbent could be a very good candidate for the separation of monovalent and divalent cations from an aqueous feed.

Finally, the recovery efficacy of IL-GO from the feed water was corroborated by a well-settled precipitation of IL-GO in aqueous solution after the adsorption of Ca^{2+} (Fig. S7). The precipitated IL-GO was easily isolated from aqueous solution through filtration. The adsorption capacity of developed IL-GO for Ca^{2+} and Mg^{2+} is compared with that of GO for Na^{+}, Ca^{2+} and Mg^{2+} (Table S2). The adsorption capacity of IL-GO for Ca^{2+} and Mg^{2+} is higher than the reported adsorption capacity of GO.

6. Adsorption Mechanism

Several factors control the adsorption capacity of an adsorbent: (i) physico-chemical properties of the adsorbents (specific surface area, porosity, pore structure); (ii) type and amount of functional moieties present on the adsorbent surface, and (iii) properties of the adsorbate [35]. The oxygen containing functional groups (C=O, C-OH and -COOH) present in GO and in the anion of IL, within the matrix of IL-GO, could be liable for different binding pathways with metal ions. GO could also form complexes with the cations because of its functional groups on the surface. Cations can interact with the aromatic structure of GO through cation-p interactions [4]. Cation-π interaction is a donor-acceptor or charge transfer interaction, which is electrostatic. The cation-π interaction energy is determined from the electronegativity of metal ions over the center of aromatic plane of GO [36]. The electronegativity describes the electron attraction capability of metal ions, which is correlated with the atom's intrinsic electronic density and distribution. The electronegativity of both ions is in the order Mg^{2+}>Ca^{2+}. Thus, adsorption of metal ions was influenced by the attraction of these metal ions with the surface of IL-GO. Another important factor for adsorption of metal ions is associated with the hydration radii of the cations. To evaluate the interaction of cations with the surface of IL-GO in aqueous solution, it is crucial to take into consideration that water is a dipole molecule, which could align around the hydrated cation through hydrogen bonding interactions. As a result, a hydration shell could be created, which shields the electronegativity of the cation causing distancing between cation and aromatic plane and, subsequently, the strength of bonding interaction is reduced [37]. The hydration radii of Ca^{2+} and Mg^{2+} are 3.13 and 3.63 Å, respectively [4]. The adsorption capacity of IL-GO was influenced together with alteration in electronegativity and hydration radii of cations (Ca^{2+} and Mg^{2+}). The electrostatic interaction between cations and the negatively charged moieties on the surface of IL-GO could have also contributed to the high adsorption of both ions. High adsorption capacity of IL-GO towards Ca^{2+} was attained due to the use of stronger binding efficacy carboxyl (-COOH) and deprotonated O-H groups with Ca^{2+} in an aqueous environment [4,8]. Moreover, the positively and negatively charged moieties of IL within IL-GO were able to attract Ca^{2+} and Mg^{2+}. The adsorption of metal ions onto the surface of IL-GO was identified by ATR-

FTIR spectra and absorption frequency of the respective peaks for IL-GO before and after Ca^{2+} or Mg^{2+} (Fig. S1 and Table S1). The peaks for C=O and C-O stretching vibrations are shifted upon adsorption of Ca^{2+} or Mg^{2+}. The C=O peak is slightly shifted from 1,560 to 1,562 cm^{-1} for Mg^{2+} and large shift in the stretching vibration of C=O peak is observed at 1,539 cm^{-1} with the adsorption of Ca^{2+}. On the other hand, the peak for C-O slightly moved from 1,376 cm^{-1} to 1,372 cm^{-1} or 373 cm^{-1} after adsorption of Ca^{2+} or Mg^{2+}. The variation in the stretching vibration of C=O and C-O peaks indicates the binding of metal ions to active sites on the surface of IL-GO through cations-complex formation with the COO^- group of IL. Additionally, the peak intensity of O-H decreased after adsorption of both cations onto the surface of IL-GO [38]. As shown in Fig. S2, 2θ value shifted from 13.76° to 13.46° for (002) plane of IL-GO with the adsorption of Ca^{2+} or Mg^{2+}. Similar findings were reported for the crosslinked GO with Ca^{2+}, Mg^{2+} or Na^+ [39]. A shift in carbon peak and its broadening are distinguished due to the change in interlayer spacing (d) between individual GO sheets after functionalization with IL as well as adsorption of metal ions. Fig. S3 to S6 present the SEM-EDX spectra of GO and IL-GO before and after adsorption of Ca^{2+} and Mg^{2+}. The characteristic peaks for elements C, O, N, S, Cl, Mn, Si, and K are spotted in SEM-EDX spectra of GO and IL-GO. An additional peak for element N in SEM-EDX spectrum of IL-GO confirms the functionalization of GO with IL and the presence of imidazolium cation within IL-GO. However, the peaks for the elements S, K, Cl, Si and Mn and Cl are observed due to the presence of impurities in GO and IL-GO samples (Fig. S3 and S4). The peaks for the element Ca and Mg are seen in SEM-EDX spectra of Ca^{2+} and Mg^{2+} adsorbed IL-GO (Fig. S5 and S6).

CONCLUSION

The current work investigated the synthesis, characterization and testing of the adsorbent IL-GO in the adsorption of Ca^{2+} and Mg^{2+} from aqueous salt solution. IL-GO with 39 wt% IL loading was produced from GO and 1-ethyl-3-methylimidazolium amino acetate via amidation and epoxide ring opening reaction. The covalently anchored IL acted as spacer between GO sheets, and more accessible active sites were created within IL-GO for adsorption. Only 2 wt% of IL leached out from IL-GO upon its immersion in DI water under continuous mechanical stirring over 24 h. The functional moieties that exist on the surface of IL-GO are responsible for improving IL-GO adsorption capacity for Ca^{2+} and Mg^{2+} ions. The adsorption of Ca^{2+} and Mg^{2+} onto IL-GO occurred through electrostatic interactions and complex formation between the cations and oxygen-containing functional moieties of IL-GO. The adsorption rates of both Ca^{2+} and Mg^{2+} followed a pseudo second-order kinetic model. The Langmuir isotherm constants were calculated from fitting the adsorption equilibrium data for both metals. The maximum adsorption capacity (q_{max}) obtained was 125 mg g^{-1} for Ca^{2+} and 73 mg g^{-1} for Mg^{2+}. Removal and recovery of IL-GO from solution after its use in adsorption was conveniently achieved through vacuum filtration. Altogether, the developed IL-GO adsorbent can efficiently remove Ca^{2+} and Mg^{2+} ions without cross-contamination of feed water with IL, while it can be easily recovered upon completion of metal ions adsorption.

ACKNOWLEDGEMENTS

The financial support by Abu Dhabi Department of Education and Knowledge (ADEK) through grant no. AARE18-019 to Ioannis Zuburtikudis of Abu Dhabi University is greatly acknowledged. The authors are thankful to Prof. Hussain Alawadhi's group at University of Sharjah, UAE for providing facilities to record Raman spectra of GO and IL-GO.

COMPLIANCE WITH ETHICAL STANDARDS

This study was funded by Abu Dhabi Department of Education and Knowledge (ADEK) through grant no. AARE18-019.

CONFLICT OF INTEREST

The authors declare that they have no conflict of interest.

SUPPORTING INFORMATION

Additional information as noted in the text. This information is available via the Internet at http://www.springer.com/chemistry/journal/11814.

REFERENCES

1. C. Q. Sun, Y. Sun, Y. G. Nie, Y. Wang, J. S. Pan, G. Ouyang, L. K. Pan and Z. Sun, *J. Phys. Chem. C*, **113**, 16464 (2009).
2. P. Bradder, S. K. Ling, S. Wang and S. Liu, *J. Chem. Eng. Data*, **56**, 138 (2010).
3. S. Stankovich, R. D. Piner, S. B. T. Nguyen and R. S. Ruoff, *Carbon*, **44**, 3342 (2006).
4. K. Yang, B. Chen, X. Zhu and B. Xing, *Environ. Sci. Technol.*, **50**, 11066 (2016).
5. F. Baskoro, C. B. Wong, S. R. Kumar, C. W. Chang, C. H. Chen, D. W. Chen and S. J. Lue, *J. Membr. Sci.*, **554**, 253 (2018).
6. A. Abusharkh, Solubility of NaCl, $MgCl_2$ and $CaCl_2$ in different ionic liquids (2015).
7. A. Terracciano, J. Zhang, C. Christodoulatos, F. Wu and X. Meng, *J. Environ. Sci.*, **57**, 8 (2017).
8. J. Shang, Y. Guo, D. He, W. Qu, Y. Tang, L. Zhou and R. Zhu, *J. Hazard. Mater.*, **416**, 125706 (2021).
9. L. Hou, C. Yang, X. Rao, L. Hu, Y. Bao, Y. Gao and X. Zhu, *Colloids Surf. A Physicochem. Eng. Asp.*, **625**, 126949 (2021).
10. R. Valavala, J. Sohn, J. Han, N. Her and Y. Yoon, *Eng. Res.*, **16**, 205 (2011).
11. R. Y. Ning, Reverse Osmosis Chemistry — Basics, Barriers and Breakthroughs, Desalination Updates. (2015). https://doi.org/10.5772/60208.
12. A. Alkhatib, M. A. Ayari and A. H. Hawari, *Chem. Eng. Process.*, **167**, 108517 (2021).
13. A. Ouadi, B. Gadenne, P. Hesemann, J. J. E. Moreau, I. Billard, C. Gaillard, S. Mekki and G. Moutiers, *Chem. Europ. J.*, **12**, 3074 (2006).

14. C. H. C. Janssen, M. C. Kroon, S. J. Metz, J. van Spronsen and G. J. Witkamp, *J. Chem. Eng. Data*, **55**, 3391 (2010).
15. L. Gholami-Bonabi, N. Ziaefar and H. Sheikhloie, *Water Sci. Technol.*, **81**, 228 (2020).
16. H. Wang and Y. Wei, *RSC Adv.*, **7**, 9079 (2017).
17. H. Yang, F. Li, C. Shan, D. Han, Q. Zhang, L. Niu and A. Ivaska, *J. Mater. Chem.*, **19** (2009).
18. D. Han and K. H. Row, *Molecules*, **15**, 2405 (2010).
19. J. Chen, B. Yao, C. Li and G. Shi, *Carbon*, **64**, 225 (2013).
20. C. Garkoti, J. Shabir, P. Gupta, M. Sharma and S. Mozumdar, *New J. Chem.*, **41** (2017).
21. H. Yang, C. Shan, F. Li, D. Han, Q. Zhang and L. Niu, *Chem. Commun.*, 3880 (2009).
22. D. R. Dreyer, S. Park, C. W. Bielawski and R. S. Ruoff, *Chem. Soc. Rev.*, **39**, 228 (2009).
23. N. R. Dhumal, H. J. Kim and J. Kiefer, *J. Phys. Chem. A.*, **113**, 10397 (2009).
24. M. Fitzpatrick, P. Champagne and M. F. Cunningham, *Carbohydr. Polym.*, **87**, 1124 (2012).
25. J. H. Kim, G. H. Shim, T. T. N. Vo, B. Kweon, K. M. Kim and H. S. Ahn, *RSC Adv.*, **11**, 3645 (2021).
26. S. Prusty, K. Pal, D. Bera, A. Paul, M. Mukherjee, F. Khan, A. Dey and S. Das, *Colloids Surf. B.*, **203**, 111729 (2021).
27. V. Georgakilas, M. Otyepka, A. B. Bourlinos, V. Chandra, N. Kim, K. C. Kemp, P. Hobza, R. Zboril and K. S. Kim, *Chem. Rev.*, **112**, 6156 (2012).
28. P. Pirkwieser, J. A. Lopez-Lopez, W. Kandioller, B. K. Keppler, C. Moreno and F. Jirsa, *Front. Chem.*, **6**, 172 (2018).
29. W. Wu, J. Wang, J. Liu, P. Chen, H. Zhang and J. Huang, *Int. J. Hydrog. Energy*, **42**, 11400 (2017).
30. I. H. Alsohaimi, S. M. Wabaidur, M. Kumar, M. A. Khan, Z. A. Alothman and M. A. Abdalla, *Chem. Eng. J.*, **270**, 9 (2015).
31. F. O. Nwosu, B. I. Olu-Owolabi and K. O. Adebowale, *Curr. Res. Chem.*, **4**(2), 26 (2012).
32. S. Prakash, M. Kumar, B. P. Tripathi and V. K. Shahi, *Chem. Eng. J.*, **162**, 28 (2010).
33. W. Plazinski and W. Rudzinski, *Langmuir*, **25**, 298 (2009).
34. X. Zhou, Y. Zhang, Z. Huang, D. Lu, A. Zhu and G. Shi, *Sci. Rep.*, **6**, 38417 (2016).
35. Q. Kong, S. Preis, L. Li, P. Luo, C. Wei, Z. Li, Y. Hu and C. Wei, *Sep. Purif. Technol.*, **232**, 115956 (2020).
36. J. C. Ma and D. A. Dougherty, *Chem. Rev.*, **97**, 1303 (1997).
37. B. Tansel, J. Sager, T. Rector, J. Garland, R. F. Strayer, L. Levine, M. Roberts, M. Hummerick and J. Bauer, *Sep. Purif. Technol.*, **51**, 40 (2006).
38. D. Gu and J. B. Fein, *Colloids Surf. A Physicochem. Eng. Asp.*, **481**, 319 (2015).
39. Y. Du, X. Zhang, J. Yang, Y. Lv, C. Zhang and Z. K. Xu, *J. Membr. Sci.*, **595**, 117586 (2020).

Supporting Information

Ionic liquid functionalized graphene oxide for the adsorption of Ca^{2+} and Mg^{2+} ions from saline aqueous feed

Botagoz Zhuman*,, Hadil Abu Khalifeh*, Ioannis Zuburtikudis*,†, Mahendra Kumar**, Hassan A. Arafat**, and Enas Nashef****

*Chemical Engineering Department, Abu Dhabi University, P.O. Box 59911, Abu Dhabi, U.A.E.
**Center for Membrane and Advanced Water Technology, Khalifa University, P.O. Box 127788, Abu Dhabi, U.A.E.
(*Received 30 July 2022 • Revised 2 December 2022 • Accepted 4 December 2022*)

Table S1. The functional groups present in GO and IL-GO based on FTIR spectra

Sample Wavelength, cm^{-1}	C=C	C=O	C-O	-OH stretch	C-O	C-O-C	C-N	N-H	C=N	C-H	C-H imidazolium ring	C-H	C-O-H
GO	1,622	1,729	1,060	3,350	1,391	1,225	-	-	-	-	-	-	-
IL	-	-	-	-	-		-	-	1,565	627	3,059	1,378	1,167
IL-GO	-	1,560	-	3,262	1,376	-	1,288	3,148	-	620	3,154	1,292	1,171
IL-GO after Ca^{2+} adsorption	-	1,539	-	3,134	1,372	-	1,261	-	-	669	-	-	1,075
IL-GO after Mg^{2+} adsorption	-	1,562	-	3,133	1,373	-	1,261	-	-	652	-	-	1,057

Table S2. Comparison of maximum adsorption capacity of IL-GO to other adsorbents reported in the literature for the adsorption of Ca^{2+} and Mg^{2+} ions

Adsorbent	Cation type	Maximum adsorption capacity (q_{max})	Conditions	Ref.
GO	Ca^{2+}	21.1 mmol g^{-1}	pH=7, GO concentration=10 mg L^{-1}, Ca^{2+}=1 mmol L^{-1}	[S1]
GO	Ca^{2+}, Na^{+}	15.3 mmol g^{-1}	pH=7, GO concentration=10 mg L^{-1}, Ca^{2+}=1 mmol L^{-1}, Na^{+}=10 mmol L^{-1} in the binary salt mixture solution	[S1]
GO	Mg^{2+}	0.95 mmol g^{-1}	pH=5, time=24 h, Mg^{2+}=2 mmol L^{-1}	[S2]
GO	Na^{+}	0.41 mmol g^{-1}	pH=5, time=24 h, Na^{+}=1.7 mmol L^{-1}	[S2]
GO	Ca^{2+}	NA	pH=6, time=24 h, Ca^{2+}=0.015 mmol L^{-1} multilayered GO concentration=210 mg L^{-1} in 0.1 M $NaClO_4$ electrolyte solution to form a parent suspension of 420 mg/L	[S3]
IL-GO	Ca^{2+}, Mg^{2+}	125 mg g^{-1} (Ca^{2+}), 73 mg g^{-1} (Mg^{2+})	pH=7, time=120 min, Ca^{2+}=130 mg L^{-1}, Mg^{2+}=140 mg L^{-1} IL-GO concentration 150 mg L^{-1}	This study

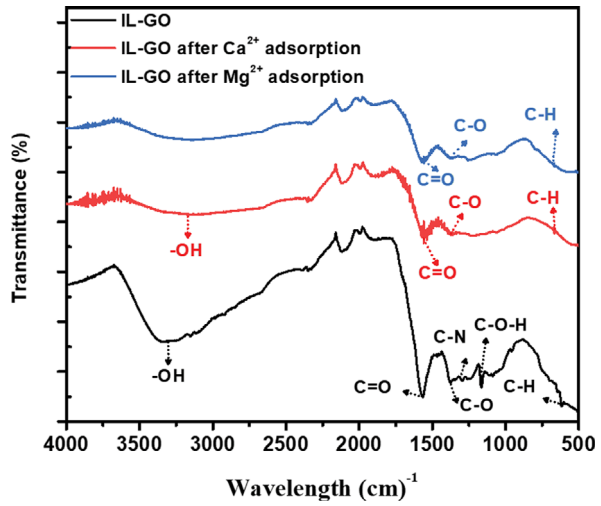

Fig. S1. ATR-FTIR spectra of IL-GO before and after Ca^{2+} and Mg^{2+} ions adsorption.

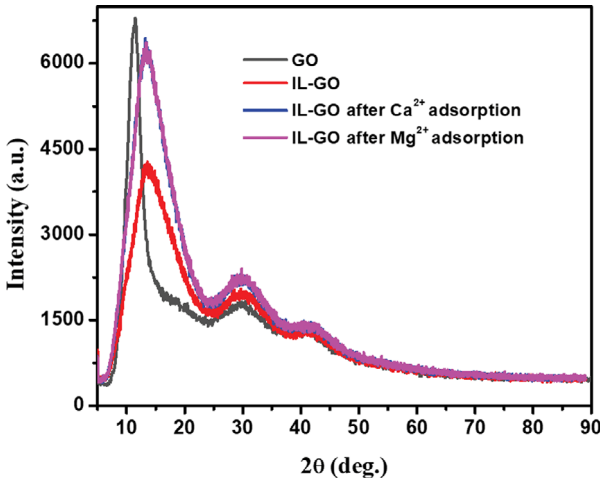

Fig. S2. WAXRD patterns of IL-GO before and after adsorption of Ca^{2+} and Mg^{2+} ions.

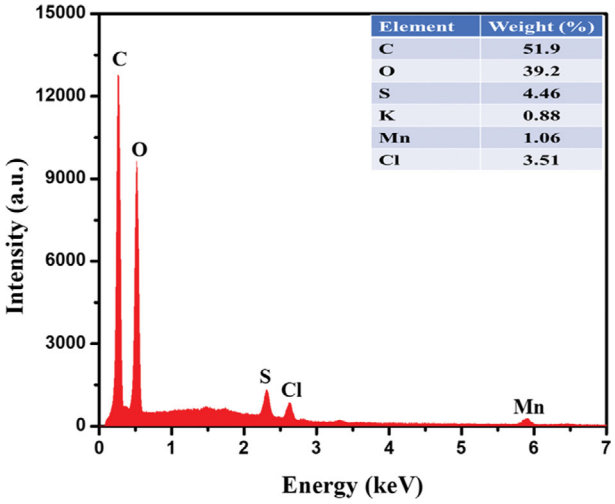

Fig. S3. SEM-EDX spectrum along with elemental composition of GO.

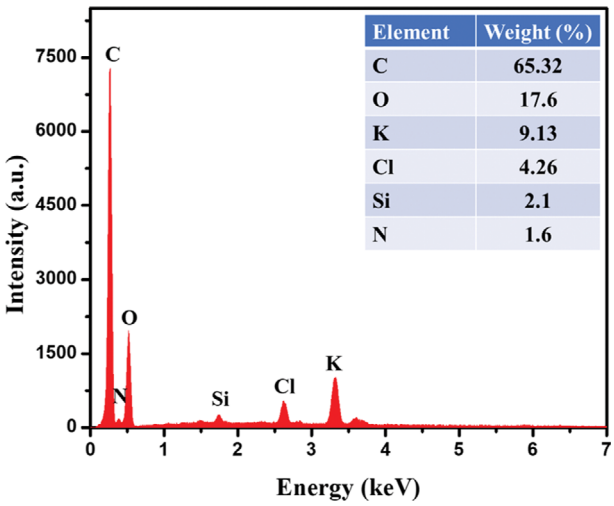

Fig. S4. SEM- EDX spectrum along with elemental composition of IL-GO.

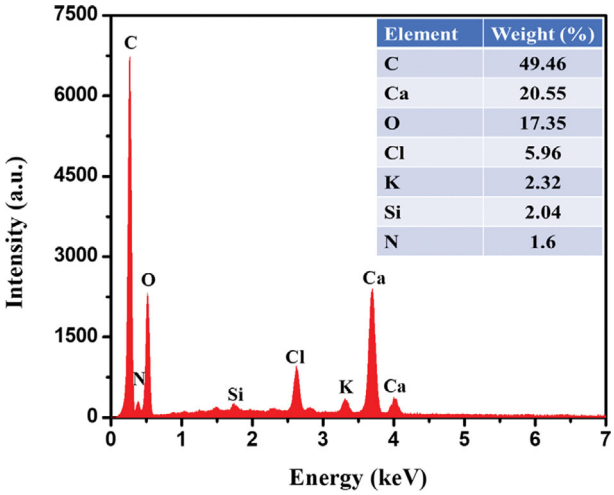

Fig. S5. SEM EDX spectrum along with elemental composition of IL-GO after Ca^{2+} adsorption.

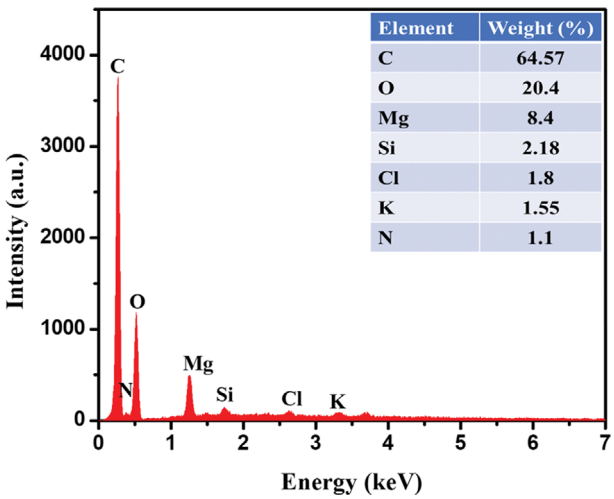

Fig. S6. SEM-EDX spectrum of along with elemental composition of IL-GO after Mg^{2+} adsorption.

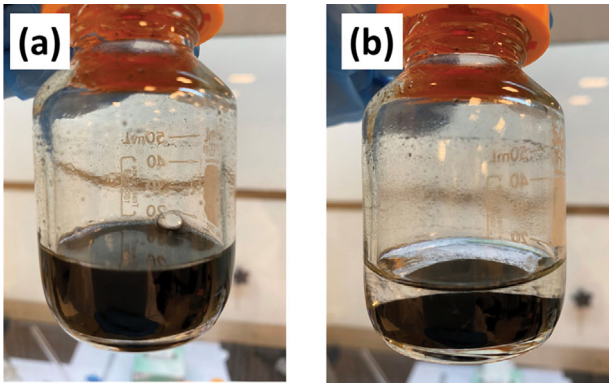

Fig. S7. Pictures of IL-GO used in the adsorption of Ca^{2+} ions in aqueous solutions before (left) and after (right) settling.

REFERENCES

1. A. Terracciano, J. Zhang, C. Christodoulatos, F. Wu and X. Meng, *J. Environment. Sci.*, **57**, 8 (2017).
2. Q. Kong, S. Preis, L. Li, P. Luo, C. Wei, Z. Li, Y. Hu and C. Wei, *Sep. Purif. Technol.*, **232**, 115956 (2020).
3. D. Gu and J. B. Fein, *Colloids Surf. A: Physicochem. Eng. Asp.*, **481**, 319 (2015).